Journal of Radiation Research, 2013, 54, 190–201
doi: 10.1093/jrr/rrs069 Advance Access Publication 14 September 2012

Source of statistical noises in the Monte Carlo sampling techniques for coherently scattered photons

Wazir MUHAMMAD[1,2] and Sang Hoon LEE[3,*]

[1]Department of Physics, Kyungpook National University, 1370 Sankyuk-dong, Buk-gu, Daegu 702-701, Korea
[2]Department of Medical Physics, Institute of Nuclear Medicine Oncology and Radiotherapy (INOR), Abbottabad, Pakistan
[3]School of Energy Engineering, Kyungpook National University, Daegu 702-701, Korea
*Corresponding author. School of Energy Engineering, Kyungpook National University, 1370 Sankyuk-dong, Buk-gu, Daegu 702-701, Korea. Tel: +82-53-950-8974 (Office); Fax: +82-53-950-8979; Email: lee@knu.ac.kr

(Received 21 March 2012; revised 12 July 2012; accepted 12 July 2012)

Detailed comparisons of the predictions of the Relativistic Form Factors (RFFs) and Modified Form Factors (MFFs) and their advantages and shortcomings in calculating elastic scattering cross sections can be found in the literature. However, the issues related to their implementation in the Monte Carlo (MC) sampling for coherently scattered photons is still under discussion. Secondly, the linear interpolation technique (LIT) is a popular method to draw the integrated values of squared RFFs/MFFs (i.e. $A(Z, v_i^2)$) over squared momentum transfer ($v_i^2 = v_1^2, \ldots\ldots, v_{59}^2$). In the current study, the role/issues of RFFs/MFFs and LIT in the MC sampling for the coherent scattering were analyzed. The results showed that the relative probability density curves sampled on the basis of MFFs are unable to reveal any extra scientific information as both the RFFs and MFFs produced the same MC sampled curves. Furthermore, no relationship was established between the multiple small peaks and irregular step shapes (i.e. statistical noise) in the PDFs and either RFFs or MFFs. In fact, the noise in the PDFs appeared due to the use of LIT. The density of the noise depends upon the interval length between two consecutive points in the input data table of $A(Z, v_i^2)$ and has no scientific background. The probability density function curves became smoother as the interval lengths were decreased. In conclusion, these statistical noises can be efficiently removed by introducing more data points in the $A(Z, v_i^2)$ data tables.

Keywords: photons' elastic (Rayleigh) scattering; Monte Carlo techniques; probability distribution Function (PDF); relativistic form factors; modified form factors

INTRODUCTION

The application of Rayleigh (elastic) scattering by bound atomic electrons as being one of the fundamental modes of photon interaction at low energy X-rays and soft γ-rays, to the different fields makes it of enhanced interest [1]. Furthermore, the availability of synchrotron sources and emerging development in the X-ray and γ-ray regime has also boosted the demand for its accurate theoretical predictions [1, 2]. In the Rayleigh scattering, the whole atom acts as a primary target for the incoming photons while the electrons of the atom must be considered bound [3–5]. The target atom that has a relatively heavy atomic mass recoils to conserve momentum before and after scattering. Due to the effectively heavy atomic mass, the photon changes its direction only with negligible energy transfer to the target atom and retains the same energy after scattering [5]. Along with the atomic Rayleigh scattering by its bound electrons, nuclear Thomson, Delbrück and nuclear resonance scattering also contribute to the elastic scattering of photons by atoms [1].

Primarily, knowledge about Rayleigh scattering of photons by bound atomic electrons can be obtained using low energy X-rays and soft γ-rays, in which the contribution from bound electrons of a neutral atom remains dominant. Now, if the electrons are considered free (i.e. bonding is neglected) the photon scattering will follow the famous Thomson scattering amplitude [6]. The differential Thomson cross-section for unpolarized photons is given by:

$$\frac{d\sigma_{th}(\theta)}{d\theta} = \frac{r_0^2}{2}(1+\cos^2\theta)2\pi\sin\theta \quad (1)$$

Here, $r_0 = 2.82 \times 10^{-13} cm$ is the classical electron radius [6, 7]. The differential cross-section for the coherent scattering may be obtained by multiplying the Thomson amplitudes and the square of the scattering atomic form factor $F(Z, E, \theta)$. The differential cross-section of coherent scattering within the atomic form factor approximation is given by:

$$\frac{d\sigma_{coh}(Z, E, \theta)}{d\theta} = \frac{d\sigma_{th}(\theta)}{d\theta} F^2(Z, E, v) \quad (2)$$

Here, Z is the atomic number of the scattering element, E is the energy of the incident photon and $v = \lambda^{-1} \sin\theta/2$ (i.e. λ (Å) is the incident photon wavelength), having units of inverse length. The $F(Z, E, v)$ can be written in terms of Relativistic Form Factors (RFFs) or Modified Form Factors (MFFs), and Anomalous Scattering Factors (ASFs) corrections as [3, 8]:

$$F^2(Z, E, v) = \{F_0(Z, v) + f'(Z, E)\}^2 + f''^2(Z, E) \quad (3)$$

Here, $F_0(Z, v)$ represents the RFF/MFF, which is the Fourier Transform of the atomic charge distribution that signifies the phase difference in scattering from the differing positions of the charge. In general, it represents the probability that the Z electrons of an atom take up the recoil momentum without absorbing any energy. It is also accounts for the effect of interfering scattering amplitudes across the atoms [4], while f' and f'' are the real and the imaginary parts of the complex scattering amplitude of the ASFs, accounting for the photoelectric influence [6, 7, 9]. The angle-independent ASFs are assumed to be isotropic and in addition, they smoothly approach zero at 1.0 MeV and, therefore, its effect can be neglected [10, 11]. Neglecting $f'(Z, E)$ and $f''(Z, E)$ in Equation (3) is considered a further acceptable approximation for the Monte Carlo (MC) sampling of angular distribution of coherently scattered photons. By using Equation (1), Equation (2) can be rewritten as:

$$\frac{d\sigma_{coh}(Z, \alpha, \theta)}{d\theta} = \frac{r_0^2}{2}(1+\cos^2\theta)2\pi\sin\theta\, F_0^2(Z, v) \quad (4)$$

The form factor, FF, (i.e. RFF/MMF) approximation is valid for photon energies much greater than the electron-binding energies. Considerable effort has been made to obtain the precise values of RFFs/MFFs. Extensive tabulations of F_0 (i.e. RFFs and MFFs) for all neutral atoms have been published in the last quarter of the 20th century [2, 5, 6, 9, 12]. These are traditionally tabulated as a function of variable v ($Å^{-1}$). The FF approximation is better justified at the energies well above the K-shell photo-effect threshold and generally gives good predictions for the total cross-sections [2, 3]. The FF approximation also works well to predict small angle differential cross-sections for the photon energies well above the K-shell photo-effect threshold. On the other hand, the effects related to atomic structure (i.e. virtual excitation and ionization of atomic electrons, at comparable energies to the atomic binding energies especially for the photon energies close to the edges) are neglected in the FF approximation. So it fails to predict any of these structures. Owing to the dominant contributions from virtual ionizations and excitations of electrons in the subshells near the edges, it performs much more poorly than for that of the other energies [2].

Franz introduced for the first time in 1936 an electron-binding correction to the atomic form factors and the resulting corrected form factors are commonly known as MFFs [1, 2, 6]. The MFFs have not been calculated directly from the total electron charge distribution like RFFs. The contribution from the electrons of each subshell of an atom have been calculated and summed. The better high-energy results for heavy elements have been produced from such calculations. Furthermore, by the introduction of electron-binding effects, the MFF approximation provides the correct relativistic high-energy limit, particularly in high-Z elements, for forward scattering. The approximation is also quite successful in reproducing Rayleigh amplitudes, even at relatively low energies, where the validity of the derivation is unclear [2, 3, 5, 6]. In general, the accuracy of the MFF increases with increasing photon energy and decreasing binding energies of the electrons [5]. Like the RFF, the MFF approximation also breaks down badly for high energy photons and at large scattering angles. However, unlike RFF, the MFF approximation gives good predictions for all elements at photon energies well above the K-shell binding after getting scattered by zero angles [3]. A complete tabulation of the MFFs values based on self-consistent relativistic wave-functions, potentials (i.e. total-atom and K-shell MFF values are listed) and by considering the spherical symmetric electronic charge distribution of the complete subshells given by Schaupp D *et al.*, for all the elements in the Periodic Table [5, 12].

Using the complete table of RFFs/MFFs covering the total energy range is almost impossible, or at least cumbersome, especially if it is included in a large production code where the speed of execution is of the primary importance. From this point of view, it is valuable to have simpler and faster methods to evaluate these data tables. The most popular method in the literature so far is the linear interpolation technique (LIT) for drawing the integrated value of squared RFFs/MFFs over squared momentum transfer (i.e. $A(Z, v_i^2)$ for $v_i^2 = v_1^2, \ldots\ldots, v_{59}^2$) using the available data tables in the code [13].

A lot of research and discussion can be found about the predictions and shortcomings of RFFs and MFFs [1, 2, 14], but here the impact of electron-binding energies on coherently scattered photons was studied using MC techniques

for the sampling of coherently scattered photons. The impact has been assessed through the application of MFFs as it has electron-binding corrections. Another reason to evaluate its impact is to produce the best fit of possible probability distribution functions (PDFs) to the real angle distribution function for the coherently scattered photons. As LIT is the most popular method of drawing the $A(Z, v_i^2)$ values for v_i^2 however, the number of data points and interval length between two consecutive data points of the $A(Z, v_i^2)$ can be an issue. Here, the factors related to the validity of LIT and the interval length between two consecutive data points of the $A(Z, v_i^2)$ have been reviewed.

MATERIALS AND METHODS

Monte Carlo simulation

In the past decades, several MC codes based on the rejection technique have been developed. The codes are either designed for the coherent scattering or for the transport of photons, containing the coherent scattering as an interaction mode of the photons. MC techniques established previously are reused in this study. [4, 7, 15].

According to these techniques, the probability of the photons scattered coherently into the polar angle interval dθ around θ is given by:

$$p(\theta)d\theta = \frac{d\sigma_{coh}(Z,E,\theta)d\theta}{\sigma_{coh}(E,\theta)} = \frac{r_0^2}{2}\frac{(1+cos^2\theta)F_0^2(v,Z)2\pi sin\theta d\theta}{\sigma_{coh}(E,\theta)} \quad (5)$$

Where, σ_{coh} is the total coherent cross section [7].

For MC purposes, let us introduce $\mu = cos\theta$ and $\alpha = E/m_0c^2$, (i.e. m_0c^2 = electron rest mass energy). Hence, the PDF in terms of μ, given in equation (5), can be written as: [4]

$$p(\mu)d\mu = \frac{d\sigma_{coh}(Z,\alpha,\mu)d\mu}{\sigma_{coh}(Z,\alpha)} \quad (6)$$

By using the trigonometric relation (i.e. $\sin^2(\theta/2) = 1/2(1-cos\theta)$) and the energy & wavelength relation, the relation, $v = \sin(\theta/2)/\lambda$ can be easily written in the following form:

$$v^2 = (k\alpha)^2(1-\mu),\ 0 \le v^2 \le \bar{v}^2 \quad (7)$$

where $k = 10^{-8}m_0c/h\sqrt{2} = 29.1445\,cm^{-1}$ and $\bar{v}^2$ corresponds to the v_{max} [13].

Equation (6) can be written as,

$$p(v^2)dv^2 = p_{coh}(\mu)\left|\frac{d\mu}{dv^2}\right|dv^2 \quad (8)$$

By using equation (7) the relations $\mu = 1 - [v^2/(k\alpha)^2]$ & $d\mu/dv^2 = -1/(k\alpha)^2$ can be easily established. Now equation (8) can be rewritten as:

$$p(v^2)dv^2 = \frac{d\sigma_{coh}(Z,\alpha,\mu)}{\sigma_{coh}(Z,\alpha)}\left|\frac{d\mu}{dv^2}\right|dv^2 = \frac{d\sigma_{coh}(Z,\alpha,\mu)}{\sigma_{coh}(Z,\alpha)}\left|-1/(k\alpha)^2\right|dv^2 \quad (9)$$

Equation (2) can be written as

$$\sigma_{coh}(Z,\alpha,\mu)d\mu = \pi r_0^2(1+\mu^2)F_0^2(Z,v)d\mu \quad (10)$$

By combining equations (9) & (10)

$$p(v^2)dv^2 = \frac{\pi r_0^2}{(k\alpha)^2\sigma_{coh}(Z,\alpha)}(1+\mu^2)F_0^2(Z,v)dv^2$$

$$\int_0^{v^2} p(v^2)dv^2 = \frac{2\pi r_0^2z^2}{(k\alpha)^2\sigma_{coh}(Z,\alpha)}\left(\frac{1+\mu^2}{2}\right) \times \int_0^{v^2}\frac{F_0^2(Z,v)}{z^2}dv^2 \quad (11)$$

Now by introducing, $A(Z,v^2) = \int_0^{v^2} F_0^2(Z,v)Z^{-2}dv^2$ and $A(Z,\bar{v}^2) = \int_0^{\bar{v}^2} F_0^2(Z,v)Z^{-2}dv^2$ for arbitrary v^2 (these values can be easily obtained by using numerical integration)equation (8) will become:

$$p(v^2)dv^2 = \frac{2\pi r_o^2z^2A(Z,\bar{v}^2)}{(k\alpha)^2\sigma_{coh}(Z,\alpha)}\left(\frac{1+\mu^2}{2}\right)\frac{F^2(Z,E,v)z^{-2}dv^2}{A(Z,\bar{v}^2)} \quad (12)$$

If, $Q(v^2) = \frac{F^2(Z,E,v)z^{-2}}{A(Z,\bar{v}^2)}$, $f(v^2) = \left(\frac{1+\mu^2}{2}\right)$ and $C_o = \frac{2\pi r_o^2z^2A(Z,\bar{v}^2)}{(k\alpha)^2\sigma_{coh}(Z,\alpha)}$, then equation (12) can be written as

$$p(v^2)dv^2 = c_0f(v^2)Q(v^2)dv^2 \quad (13)$$

To assign v^2 with density $Q(v^2)$, a random number ξ on (0 to 1) can therefore be used as follows [4, 7]:

$$\xi = \int_0^{v^2} Q(v^2)dv^2 = A(Z,E,v^2)/\overline{A}(Z,E,\bar{v}^2) \quad (14)$$

The value of v^2 being accepted with probability [4, 7]:

$$f(v^2) = \frac{(1+\mu^2)}{2} \le 1 \quad (15)$$

The integrated values of squared MFFs (i.e. $A_{MFF}(Z,v_i^2)$)

and squared RFFs (i.e. $A_{RFF}(Z,v_i^2)$) over v^2 for $v_i^2 = v_1^2, \ldots\ldots, v_{25}^2/v_{53/59}^2/v_{85}^2$ has been calculated for hydrogen (H, Z = 1) H-1, Germanium (Ge, Z = 32) Ge-32 and Lead (Pb, Z = 82) Pb-82 by numerical integration [4, 7]. The percentage differences in $A_{MFF}(Z,v_i^2)$ and $A_{RFF}(Z,v_i^2)$ for $v_i^2 = v_1^2, \ldots\ldots, v_{59}^2$ for H-1, Ge-32 and Pb-82 were calculated using the following relation:

$$\%\,\text{difference} = \frac{\left(A_{RFF}(Z,v_i^2) - A_{MFF}(Z,v_i^2)\right)}{\{(A_{RFF}(Z,v_i^2) + A_{MFF}(Z,v_i^2))/2\}} \times 100 \quad (17)$$

To find the impact of the electron-binding correction on the angular distribution of -scattered photons, first the tabulated values of $A_{RFF}(Z,v_i^2)$ for $v_i^2 = v_1^2, \ldots\ldots, v_{59}^2$, were included in the simulation code of coherent scattering. In the second step, the tabulated values of $A_{RFF}(Z,v_i^2)$ were replaced by $A_{MFF}(Z,v_i^2)$ for $v_i^2 = v_1^2, \ldots\ldots, v_{59}^2$ (i.e. those consider the electron-binding energies) [2] in the simulation code. In both cases the PDFs were constructed through the above-mentioned MC techniques. During the program execution, the required $A(Z,v_i^2)$ values and v^2 values can be found out through LIT by using the available input data tables of the $A_{MFF}(Z,v_i^2)/A_{RFF}(Z,v_i^2)$ for $v_i^2 = v_1^2, \ldots\ldots, v_{25}^2/v_{53/59}^2/v_{85}^2$ inside the code [4, 7]. The validity/effects of LIT on the MC sampling for the coherent scattering and the interval length between two adjacent data points of $A_{MFF}(Z,v_i^2)$ in its input data tables were also analysed. In doing so, 25 ($n = 25$), 53 ($n = 53$) and 85 ($n = 85$) data points of MFF for 'v' from 0 to 16.0 Å^{-1} were used to calculate $A_{MFF}(Z,v_i^2)$ for $v_i^2 = v_1^2, \ldots\ldots, v_{25}^2/v_{53}^2/v_{85}^2$. On the basis of these values, the PDFs have been constructed through our MC code. The study was performed for H-1, Ge-32 and Pb-82 to find out the relation of the electron-binding correction and the interval length effect to atomic number (i.e. Z).

RESULTS AND DISCUSSION

The calculated values of $A_{MFF}(Z, v_i^2)$ and $A_{RFF}(Z, v_i^2)$ (i.e. for $v_i^2 = v_1^2, \ldots\ldots, v_{59}^2$) for H-1, Ge-32 and Pb-82 are presented in Fig. 1a–c. The figure shows that $A_{MFF}(Z,v_i^2)$ have smaller values compared to $A_{RFF}(Z,v_i^2)$ for Ge-32 and Pb-82, while the reverse is true for H-1. However, in both cases, the difference appears to increase for a while and then become constant. The mean, standard deviation (SD), minimum and maximum were calculated in the percentage differences of $A_{MFF}(Z,v_i^2)$ and $A_{RFF}(Z,v_i^2)$ for H-1, Ge-32 and Pb-82. The results have been summarized in Table 1. The mean values, $-2.138\,51 \pm 0.924\,88$, $1.050\,46 \pm 0.515\,04$ and $2.005\,74 \pm 0.193\,71$, have been reported for H-1, Ge-32 and Pb-82, respectively (see Table 1). Fig. 1d shows the mean of the % differences between $v_i^2 = 0, \ldots\ldots, v_{59}^2$ and $A_{RFF}(Z,v_i^2)$ for $v_i^2 = 0, \ldots\ldots, v_{59}^2$ for H-1, Ge-32 and Pb-82.

Figure 2a–f shows the sampled relative probability density based on $A_{MFF}(Z,v_i^2)$ and $A_{RFF}(Z,v_i^2)$ with $v_i^2 = v_1^2, \ldots\ldots, v_{59}^2$, for the photons, having 0.001 MeV and 0.005 MeV energies after getting scattered by H-1, Ge-32 and Pb-82. The inset of Fig. 2a–f shows the magnified view of the relative probability densities of the angular distribution of the scattered photons for a specific range of μ. In the magnified views, the difference between the curves, constructed using RFFs and MFFs, can be observed for both energies. The difference is more visible for 0.001 MeV compared to 0.005 MeV and looks most prominent in case of H-1. Fig. 3a–f shows the relative probability density for the photons having 0.01 MeV and 0.05 MeV energies after getting scattered by H-1, Ge-32 and Pb-82. Here, the difference between the scattered angle distribution using $A_{MFF}(Z,v_i^2)$ and $A_{RFF}(Z,v_i^2)$ is only visible for H-1 at 0.01 MeV. Similarly, Fig. 4a–f shows the relative probability density for the photons having 0.1 MeV and 0.5 MeV energies. There is no distinguishable difference between the scattered angular distribution using $A_{MFF}(Z,v_i^2)$ versus $A_{RFF}(Z,v_i^2)$ on the scale of this plot, as can be observed from the insets of this figure. In general, it has been found that the inclusion of electron-binding energies makes some effect on relative probability densities at low energy, and as the energy of the photon increases the difference decreases. At high energy (i.e. >1 MeV) they are indistinguishable. It has also been found that in case of light elements like H-1, the difference is more visible compared to high Z elements, i.e. Pb-82. However, the literature has considered the MFFs as an improved approximation of exact scattering amplitudes, as long as the MFFs and RFFs are of the same order of magnitude and at large scattering angles [5]. Nevertheless, the results reveal that the difference between sampled angular distribution using $A_{MFF}(Z,v_i^2)$ and $A_{RFF}(Z,v_i^2)$ is very small in the energy range ~0.001–0.5 MeV. No extra information was obtained using MFFs instead of RFFs in the sampling of PDFs for coherent scattering in this energy range.

In Figs 2–4, non-smooth curves with multiple small peaks and irregular/step shapes, more prominent for the low energies, have been produced. The relation of these multiple small peaks and irregular/step shapes to MFFs/RFFs and Z were investigated from the results obtained. These shapes were present in the relative probability density curves constructed using both the $A_{MFF}(Z,v_i^2)$ and $A_{RFF}(Z,v_i^2)$ for all the elements under the study, and hence their interconnection has been ruled out. Next, its relation with the MC techniques used for the sampling of coherently scattered photons was investigated. These may be appeared due to some shortcomings in the MC techniques and are considered as statistical noise in the PDFs. It is a

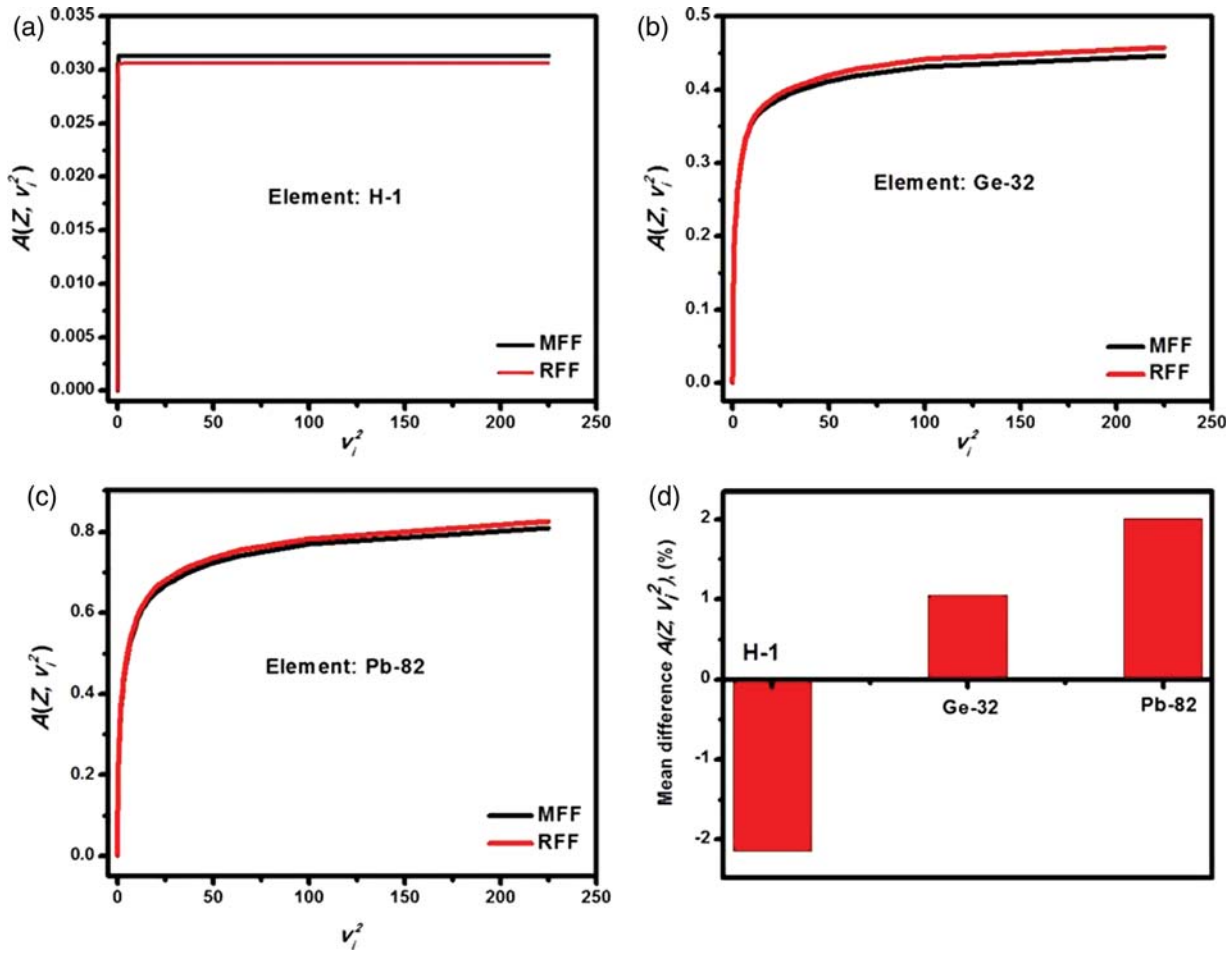

Fig. 1. $A_{MFF}(Z, v_i^2)$ and $A_{RFF}(Z, v_i^2)$ for $v_i^2 = 0, \ldots\ldots, v_{s59}^2$ calculated on bases of MFF and RFF respectively for (**a**) hydrogen (H, Z = 1), (**b**) Germanium (Ge, Z = 32), (**c**) Lead (Pb, Z = 82), (**d**) mean difference in % of $A_{MFF}(Z, v_i^2)$ and $A_{RFF}(Z, v_i^2)$ hydrogen (H, Z = 1), Germanium (Ge, Z = 32) and Lead (Pb, Z = 82).

well-known fact that a random number generator (RNG) is at the heart of MC techniques. However, no relationship was found between the noise and either the RNG or the number of the simulated photons.

The next step was to find out the relationship of these multiple small peaks and irregular/step shapes with the LIT used inside the MC code. For this purpose, the relative probability density was sampled for 25 ($n = 25$), 53 ($n = 53$) and 85 ($n = 85$) data points of $A_{MFF}(Z, v_i^2)$ for the 'v' in the range ~ 0–16.0 Å^{-1}. The MC samplings were performed for photons of energy in the range ~0.0025–0.01 MeV after getting scattered by H-1, Ge-32 and Pb-82. Figure 5a–d shows the relative probability density for the photons, having 0.0025 MeV, 0.005 MeV, 0.0075 MeV and 0.01 MeV energies by using $n = 25$, $n = 53$ and $n = 85$ for H-1. The difference can be seen between the curves, constructed by using $A_{MFF}(Z, v_i^2)$ based on $n = 25$, $n = 53$ and $n = 85$ for all the energies in the study. The difference is most prominent for $n = 25$ having some irregular shapes. These irregular shapes at $n = 25$ are converted to the step shapes for $n = 53$ while the density of these shapes was further reduced for $n = 85$ at 0.0025 MeV. Figure 5a–d shows that as the photon energy was increased from 0.0025 MeV to 0.01 MeV, the density of the step shapes apparently decreased, but in fact the decrease was not related to the energy but to the difference in the plot scale for different energies. Meaningful results

Table 1. Mean, Standard Deviation (SD), Minimum and Maximum of percentage difference of $A_{MFF}(Z, v_i^2)$ and $A_{RFF}(Z, v_i^2)$ for $v_i^2 = 0, \ldots\ldots, v_{59}^2$ calculated on bases MFF and RFF respectively.

Element	Mean ± SD	Minimum	Maximum
H-1	–2.138 51 ± 0.924 88	–3.533 23	0.004 22
Ge-32	1.050 46 ± 0.515 04	0.530 29	2.506 37
Pb-82	2.005 74 ± 0.193 71	1.583 21	2.432 69

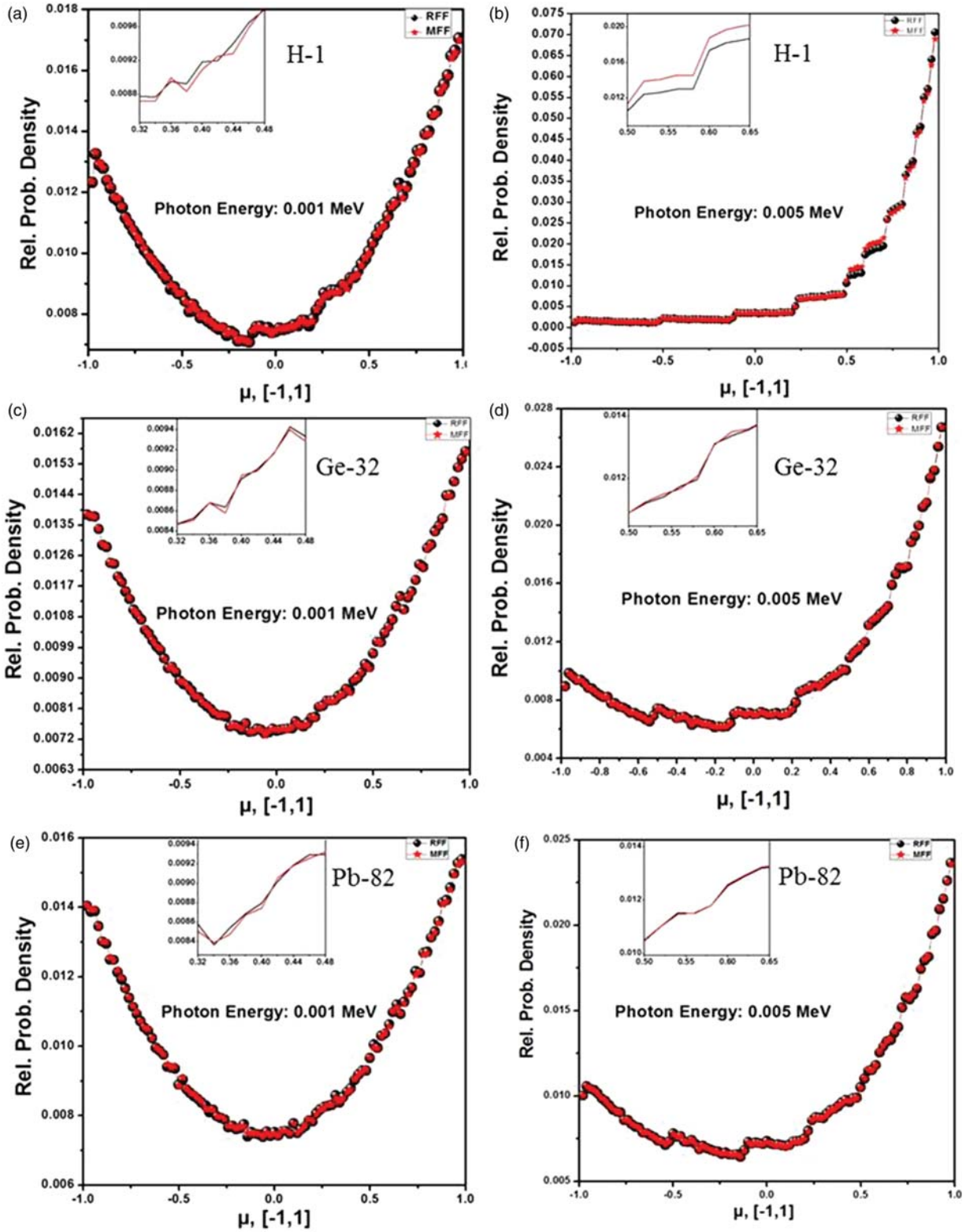

Fig. 2. Angle distribution of coherently scattered photon for source of 1 million photons. Inset shows the magnified view of relative probability density in the specific μ (i.e. cosθ) range. (**a**) Scatter element = H, energy = 0.001 MeV, (**b**) Scatter element = H, energy = 0.005 MeV, (**c**) Scatter element = Ge, energy = 0.001 MeV, (**d**) Scatter element = Ge, energy = 0.005 MeV, (**e**) Scatter element = Pb, energy = 0.001 MeV, (**f**) Scatter element = Pb, energy = 0.005 MeV.

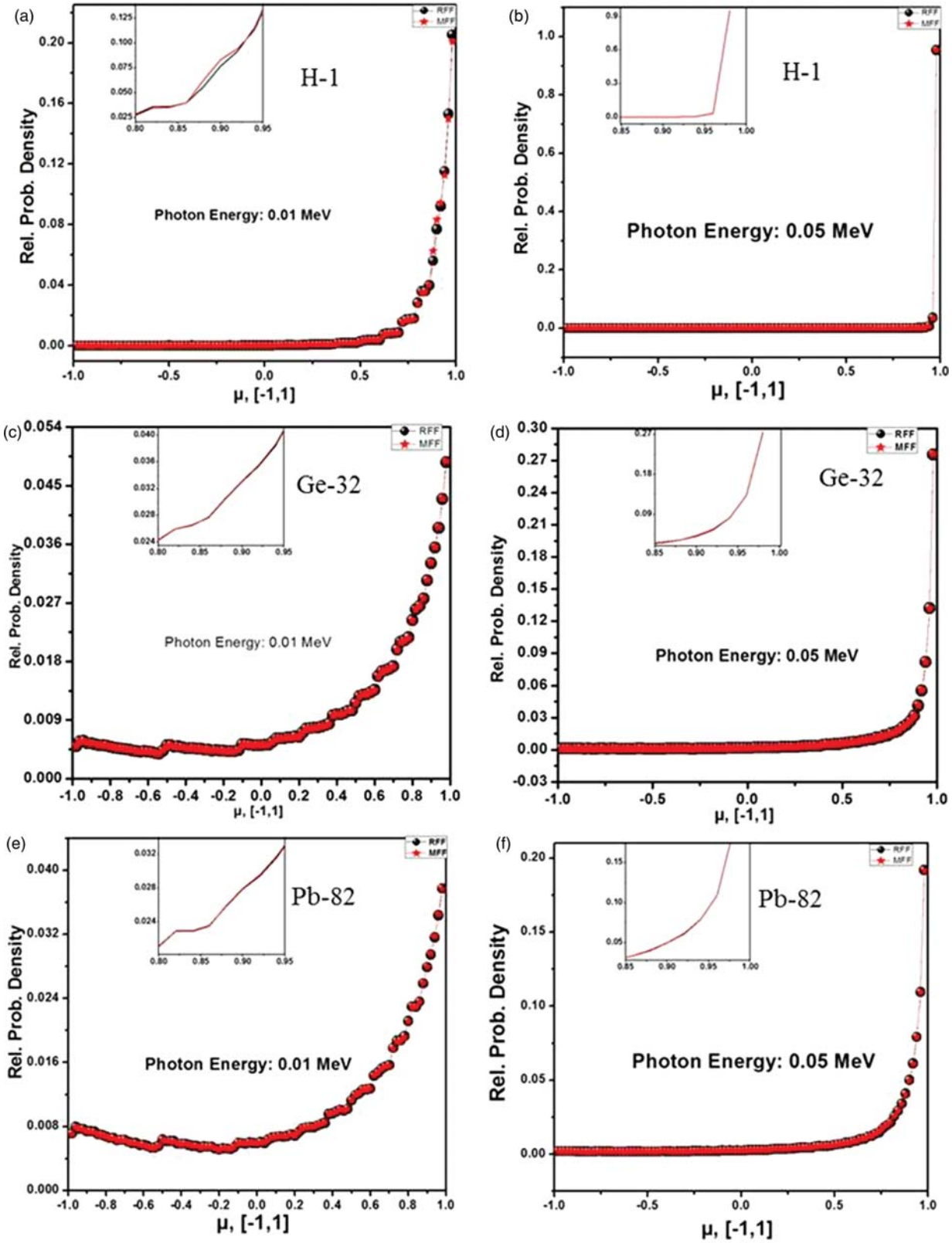

Fig. 3. Angle distribution of coherently scattered photon for source of 1 million photons. Inset shows the magnified view of relative probability density in the specific μ (i.e. cosθ) range. (**a**) Scatter element = H, energy = 0.01 MeV, (**b**) Scatter element = H, energy = 0.05 MeV, (**c**) Scatter element = Ge, energy = 0.01 MeV, (**d**) Scatter element = Ge, energy = 0.05 MeV, (**e**) Scatter element = Pb, energy = 0.01 MeV, (**f**) Scatter element = Pb, energy = 0.05 MeV.

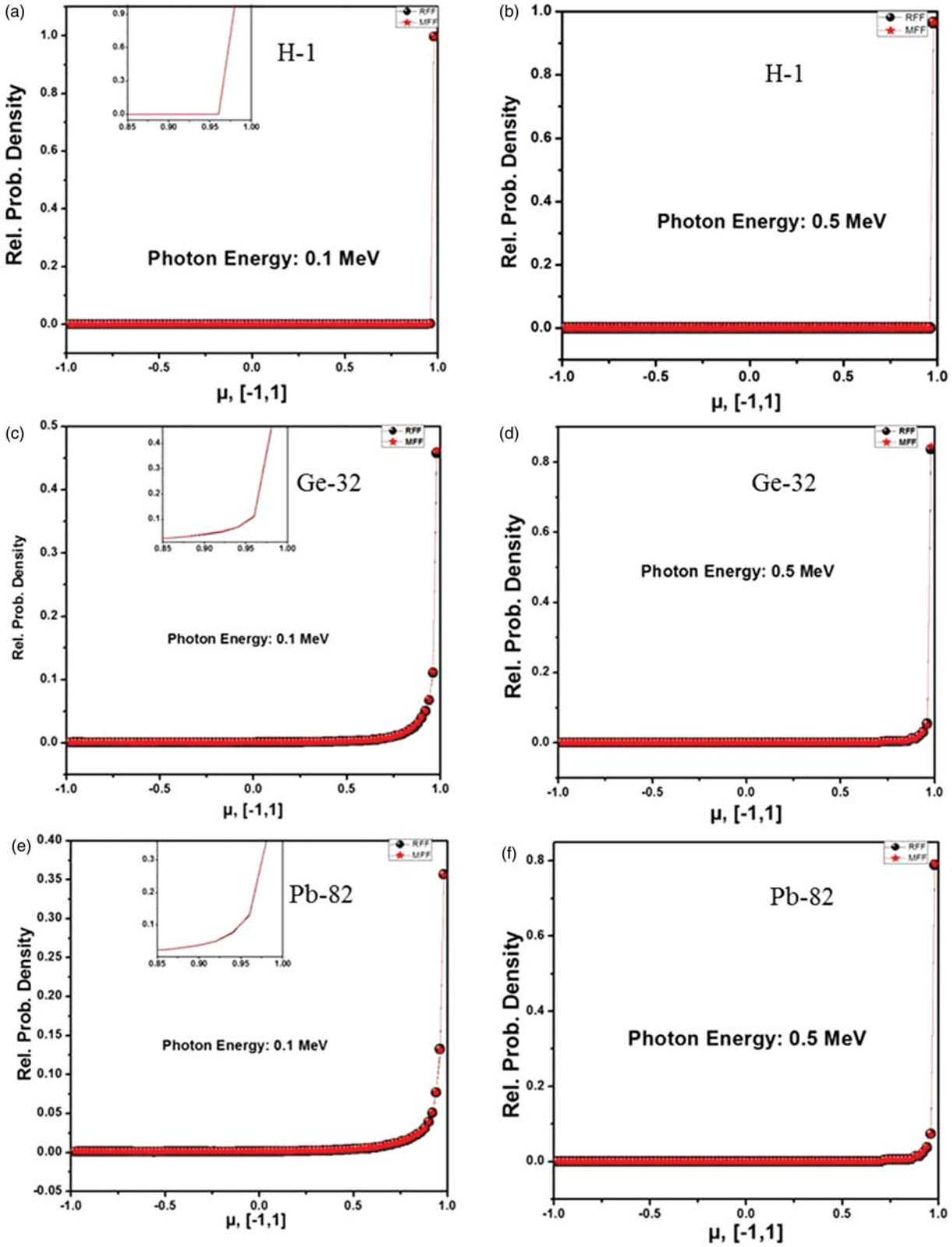

Fig. 4. Angle distribution of coherently scattered photon for source of 1 million photons. Inset shows the magnified view of relative probability density in the specific μ (i.e. cosθ) range. (**a**) Scatter element = H, energy = 0.1 MeV, (**b**) Scatter element = H, energy = 0.5 MeV, (**c**) Scatter element = Ge, energy = 0.1 MeV, (**d**) Scatter element = Ge, energy = 0.5 MeV, (**e**) Scatter element = Pb, energy = 0.1 MeV, (**f**) Scatter element = Pb, energy = 0.5 MeV.

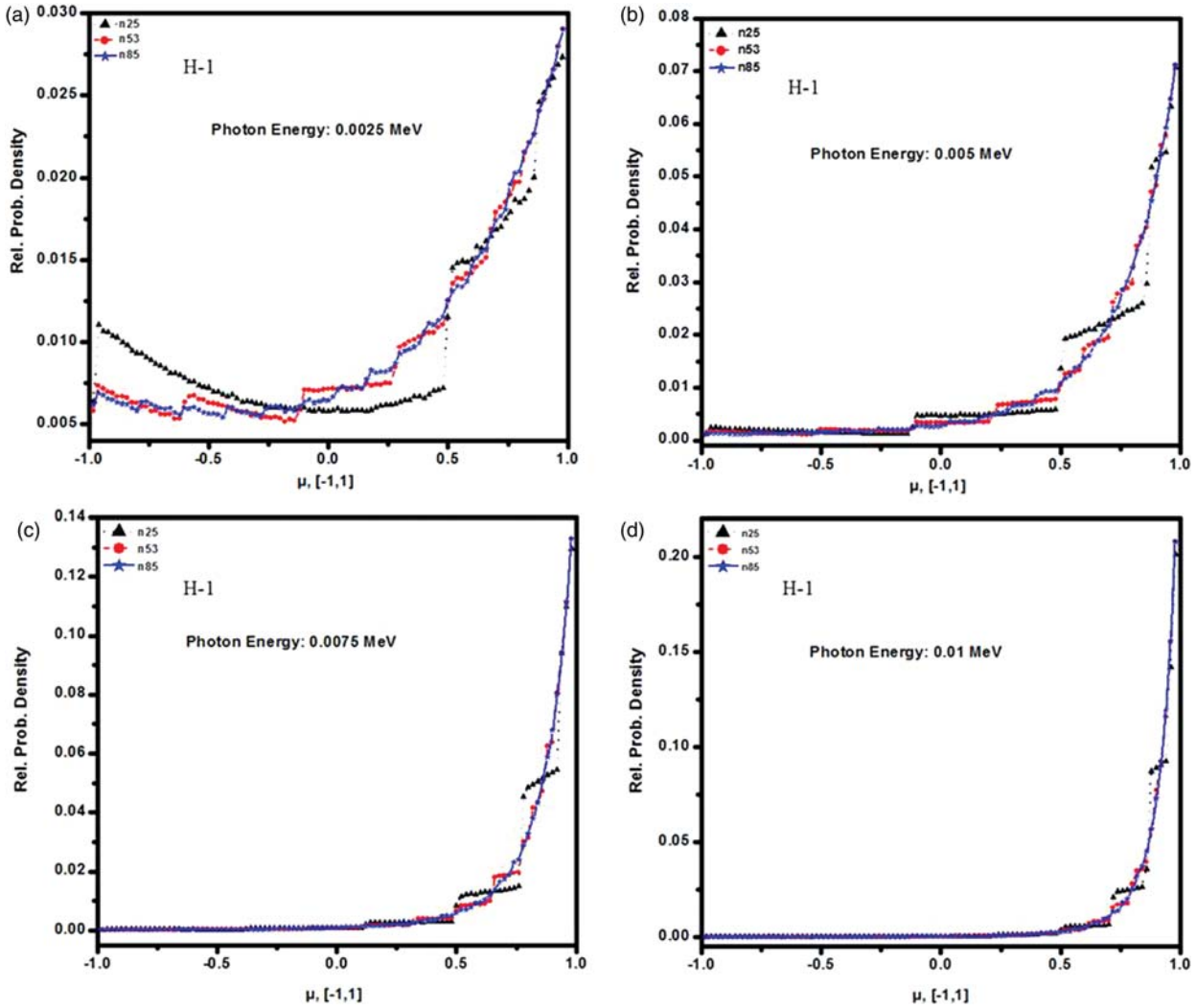

Fig. 5. Angle distribution of coherently scattered photon for source of 1 million photons by using 25 ($n = 25$), 53 ($n = 53$) and 85 ($n = 85$) data points of AFF for 'v' from 0 to 16.0 $Å^{-1}$ for H as a scatter element. (**a**) energy = 0.0025 MeV, (**b**) energy = 0.005 MeV, (**c**) energy = 0.0075 MeV, (**d**) energy = 0.01 MeV.

can be obtained by inter-compression of the curves sampled on the basis of $n = 25$, $n = 53$ and $n = 85$ at the same energy. As a result, a clear difference can be seen between the curves sampled on the basis of $n = 25$, $n = 53$ and $n = 85$. Similarly, Fig. 6a–d shows the probability densities for scattered photons, having 0.0025 MeV, 0.005 MeV, 0.0075 MeV and 0.01 MeV energies for Ge-32 as a scattering element, while Fig. 7a–d shows the probability densities for the scattered photons, having 0.005 MeV, 0.0075 MeV, 0.01 MeV and 0.05 MeV energies for Pb-82 as a scattering element by using $A_{MFF}\left(Z, v_i^2\right)$ based on $n = 25$, $n = 53$ and $n = 85$ respectively. Like Fig. 5a–d, the same pattern has been observed but the difference between $n = 25$, $n = 53$ and $n = 85$ was decreased as Z for the scattering element was increased (i.e. Ge-32 and Pb-82) in the same range of energy. Now, it is clear from these figures that these multiple small peaks and irregular/step shapes are related to LIT. As the interval length between the two consecutive data points of $A_{MFF}\left(Z, v_i^2\right)$ was reduced, the density of multiple small peaks and irregular/step shapes in the probability density function was also reduced. Finally, it can be concluded that the multiple small peaks and irregular/step shapes depend upon the interval length between the two consecutive data points of $A_{MFF}\left(Z, v_i^2\right)$ in the input data tables. As the interval length increases, the shapes density in the relative probability density curves for the scattered photons increases, and the curve becomes smoother as the interval lengths are decreased. A smooth curve is expected if a large number of data points with the

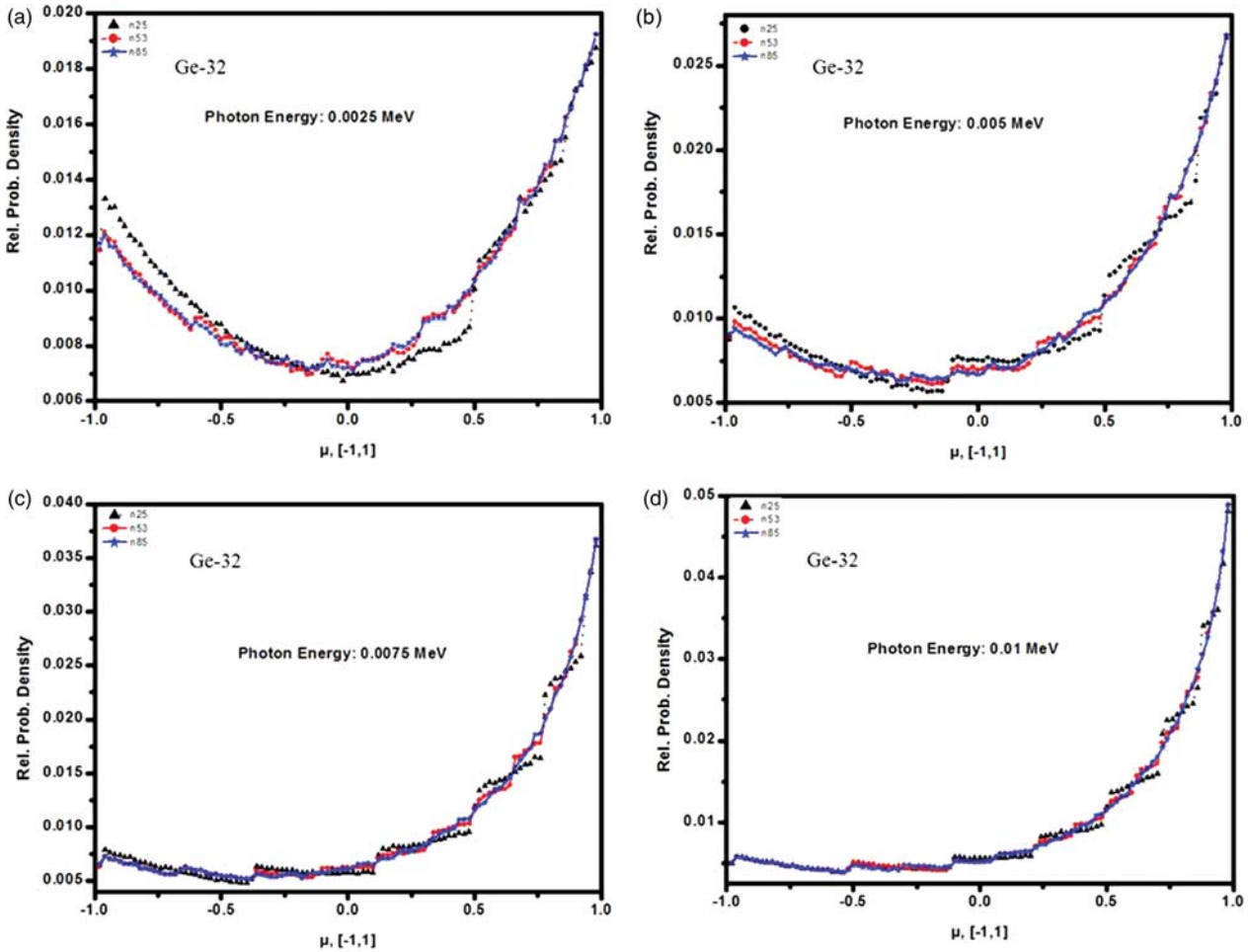

Fig. 6. Angle distribution of coherently scattered photon for source of 1 million photons by using 25 ($n = 25$), 53 ($n = 53$) and 85 ($n = 85$) data points of AFF for 'v' from 0 to 16.0 $Å^{-1}$ for Ge as a scatter element. (**a**) energy = 0.0025 MeV, (**b**) energy = 0.005 MeV, (**c**) energy = 0.0075 MeV, (**d**) energy = 0.01 MeV.

smallest possible interval lengths are included in the code. Furthermore, these can be considered as a statistical noise in the PDFs because of their relationship to sampling techniques rather than scientific background.

CONCLUSION

In conclusion, the MFFs had some effect, more visible for low Z than high Z elements, on relative probability densities at low energy. However, the effect is very small and both RFFs and MFFs produced the same MC sampled angular distribution results for coherently scattered photons. No extra information was revealed by using MFFs instead of RFFs. Both can be used for the general purpose MC simulation of coherently scattered photons. Furthermore, no relationship was established between the multiple small peaks and irregular/step shapes in the PDFs either with RFFs or MFFs, as a result their scientific background has been ruled out. In fact, these appeared to be due to the use of LIT inside the MC sampling and can be treated as statistical noise in the PDFs. The interval length between two consecutive points in the input data tables of $A(Z, v_i^2)$ increases as the density of the noise increases and vice-versa. Furthermore, it can be concluded that a smooth curve can be produced if a large number of data points with the smallest possible interval length are used in the code. Therefore, to remove the statistical noise, the introduction of more data points with smaller interval lengths between two consecutive points in the input data tables of $A(Z, v_i^2)$ can be an efficient tool.

FUNDING

This research was financially supported by the Ministry of Education, Science Technology (MEST) and the National Research Foundation of Korea (NRF) through the Human

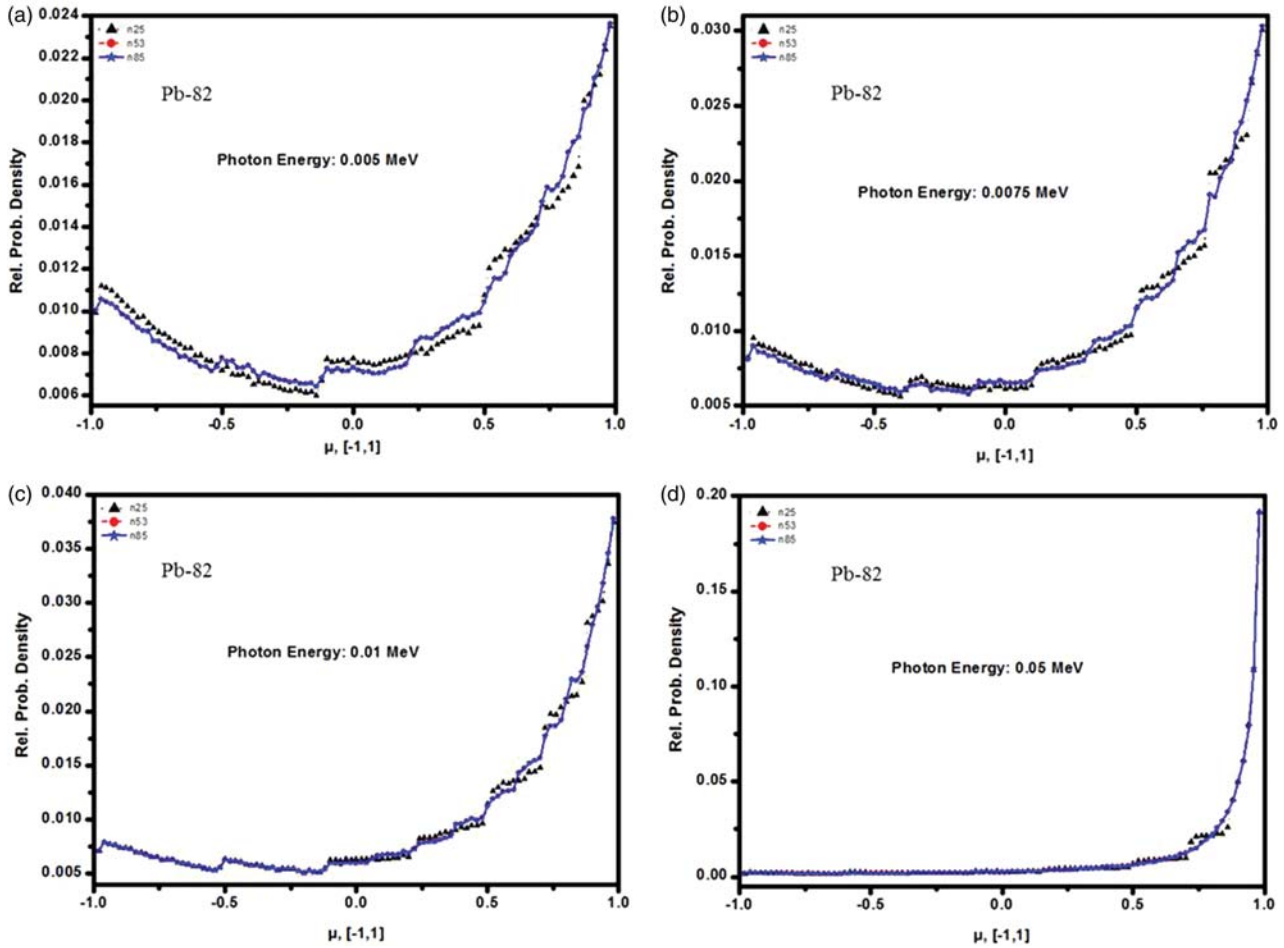

Fig. 7. Angle distribution of coherently scattered photon for source of 1 million photons by using 25 ($n = 25$), 53 ($n = 53$) and 85 ($n = 85$) data points of AFF for 'v' from 0 to 16.0 $Å^{-1}$ for Pb as a scatter element. (**a**) energy = 0.005 MeV, (**b**) energy = 0.0075 MeV, (**c**) energy = 0.01 MeV, (**d**) energy = 0.05 MeV.

Resource Training Project for Regional Innovation (2012H1B8A2026280) and by the second stage of the Brain Korea 21 Project in 2012.

REFERENCES

1. Roy SC, Pratt RH, Kissel L. Rayleigh scattering by energetic photons: Development of theory and current status. *Radiat Phys Chem* 1993;**41**:725–38.
2. Kissel L, Zhou B, Roy SC *et al*. The validity of form-factor, modified form-factor and anomalous-scattering-factor approximations in elastic scattering calculations. *Acta Cryst* 1995; **A51**:271–88.
3. Roy SC, Kissel L, Pratt RH. Elastic scattering of photons. *Radiat Phys Chem* 1999;**56**:3–26.
4. Carter LL, Cashwell ED. Particle transport simulation with the Monte Carlo method, Los Alamos Scientific Laboratory. Technical Information Center, Office of Public Affairs U. S. Energy Research and Development Administration, 1975.
5. Schaupp D, Schumacher M, Smend F *et al*. Small-angle Rayleigh scattering of photons at high energies: Tabulations of relativistic HFS modified atomic form factors. *J Phys Chem Ref Data* 1983;**12**:467–508.
6. Kane PP, Kissel L, Pratt RH *et al*. Elastic scattering of y-rays and X-rays by atoms. *Phys Rep* 1986;**140**:75–159.
7. Persliden J. A Monte Carlo program for photon transport using analogue sampling of scattering angle in coherent and incoherent scattering processes. *Comput Prog Biomed* 1983;**17**:115–28.
8. Bergstrom PM, Jr, Kissel L, Pratt RH *et al*. Investigation of the angle dependence of the photon-atom anomalous scattering factors. *Acta Cryst* 1997;**A53**:7–14.
9. Tartari A, Taibi A, Bonifazzi C *et al*. Updating of form factor tabulations for coherent scattering of photons in tissues. *Phys Med Biol* 2002;**47**:163–75.
10. Cullen DE. A simple model of photon transport. *Nucl Instrum Meth B* 1995;**101**:499–510.
11. Cullen DE, Perkins ST, Seltzer SM. Photon and electron data bases and their use in radiation transport calculations. *Appl Radiat Isot* 1993;**44**:1343–7.

12. Hubbell JH, Øverbø I. Relativistic atomic form factors and photon coherent scattering cross sections. *J Phys Chem Ref Data* 1979;**8**:69–105.
13. X-5 Monte Carlo Team. MCNP – A General Monte Carlo N-Particle Transport Code, Version 5, Vol. I: Overview and Theory, 2003.
14. Pratt RH, Kissel L, Bergstrom PM, Jr. New relativistic S-Matrix results for scattering - beyond the usual anomalous factors/beyond impulse approximation. In: Materlik G, Sparks CJ, Fischer K (eds). *Resonant Anomalous X-Ray Scattering*. Amsterdam: Elsevier Science, 1994, 9–33.
15. Kawrakow I, Mainegra-Hing E, Rogers DWO *et al*. The EGSnrc code system: Monte Carlo simulation of electron and photon transport. *NRCC Report PIRS-701*, 2010. 315 pp.